www.rericjournal.ait.ac.th

Scattering Dynamics in Thermal Environments Around PEMFC Electrode

S.H. Dhobi*, [1], S.P. Gupta^, K. Yadav^, and A.K. Jha[#]

Abstract – *The study of scattering dynamics in thermal environments around Proton Exchange Membrane Fuel Cell (PEMFC) electrode is crucial for understanding the behavior of charge carriers and the impact of thermal gradients on fuel cell performance. The aim of this work is to develop theoretical model of the Differential Cross Section (DCS) around the anode of PEMFC, focusing on electron interactions within thermal environment generated during H_2/Pt reactions. The developed theoretical model, explores the DCS dynamics under varied parameters such as scattering angles, incident electron energies, separation distances between target and incident electrons, considering both temperature effects and their absence. The findings unveil intricate DCS patterns across diverse conditions, offering significant insights into PEMFC efficiency and performance. On comparisons across three polarization scenarios reveal distinctive DCS trends, with linear polarization exhibiting lower values compared to circular, and circular polarization lower than elliptical, concerning scattering angle, energy, and distance separation. Moreover, the study investigates the interplay between DCS and PEMFC current production, the interaction between quantum species formation around electrode resultant output current. The computed of model highlight the influence of interaction surface size, charge analysis, and electrode current density on DCS behavior, providing pathways for optimizing PEMFC performance. Additionally, the study examines temperature variations within PEMFC in relation to current density and surface area. The results underscore complex relationships between these factors, emphasizing their implications for thermal management strategies in PEMFC design. Overall, this study offers comprehensive insights into the intricate dynamics of DCS within PEMFC, furnishing valuable guidance for enhancing PEMFC efficiency and performance across diverse operational contexts.*

Keywords – PEMFC, Differential Cross Section (DCS), Electron interactions, Thermal environment, Efficiency.

1. INTRODUCTION

A PEMFC is an electrochemical device that converts chemical energy from hydrogen fuel into electrical energy through a process involving protons (H^+), electrons, and oxygen. It consists of an anode, a cathode, and a proton-conducting polymer membrane (the electrolyte). Hydrogen is supplied at the anode, where it splits into protons and electrons. The protons pass through the membrane, while the electrons travel through an external circuit, generating an electric current. At the cathode, protons and electrons combine with oxygen to form water. PEMFCs are known for their high efficiency, low operating temperature (typically between 60°C and 100°C), and low emissions, making them suitable for applications in transportation, portable power, and stationary power generation. In the context of scattering under the influence of a laser field, the DCS refers to the probability distribution of particles being scattered at specific angles and energy states when subjected to a laser's electromagnetic field. When particles such as electrons, protons, or atoms scatter in the presence of a laser, the laser field can interact with the particles and alter their trajectories and energy states through photon absorption or emission processes. The DCS in the presence of a laser field helps describe how the scattering of particles is influenced by the laser, providing insights into the interaction dynamics between the particles and the electromagnetic field.

Dhobi *et al*. analyse the thermodynamic properties of thermal electrons involved in scattering events, filling a gap in previous research in which such interactions involving thermal electrons within the context of the laser field have never been adequately investigated. By modelling the thermal Hamiltonian within the context of the laser field, the investigation uses the partition function to investigate these thermodynamic features, providing insights into the difficulties of DCS determinations [1]. Banerji and Mittleman explored the elastic scattering of electrons via hydrogen atoms in the context of linearly polarised strong lasers, revealing considerable differences in their laser-modified DCS from previous findings [2]. Furthermore, Bhattacharya *et al*. investigated the elastic scattering of electrons via hydrogen atoms in the presence of two linearly polarised laser fields, providing knowledge about the DCS results' dependency on different geometrical configurations along with laser field characteristics [3]. Dahiri *et al*. analyzed electron-nucleon scattering processes in the presence of circularly polarized electromagnetic pulses, revealing

*Central Department of Physics, Tribhuvan University, Kirtipur 44618, Nepal.

^Department of Physics, Patan Multiple Campus, Tribhuvan University, Lalitpur 44700, Nepal.

[#]Department of Mechanical and Advance Engineering, Institute of Engineering, Pulchowk Campus, Tribhuvan University, Lalitpur 44700, Nepal.

[1]Corresponding authors: saddam@ran.edu.np; yadavkishori70@gmail.com

reductions in the differential cross-section and form factor when laser fields are applied, while providing comparative insights between electron-proton and electron-neutron scattering scenarios [4]. This research does not explore the interactions between quantum species in an environment created by self-generated thermal radiation. Previous studies have used artificial lasers to perturb the system. However, in this research, the system is perturbed by the self-energy generated by the exothermic reaction, where the energy produced is in the form of heat, considered as IR frequency or an IR laser field. The perturbed system in this study is self-created by the exothermic reaction inside the PEMFC.

In contrast, artificial laser-assisted scattering, which has evolved since the 1960s, with seminal theories proposed by Kroll and Watson, and Byron and Joachain, has led to the development of numerous models. However, these theories and models have largely overlooked the thermal dynamics of scattering systems, particularly interactions involving electrons and atoms in a thermal environment. A critical gap in the literature concerning thermal cases was identified, which was addressed in 2020 by Dhobi *et al.*, who formulated a thermal wave function for electrons in a linearly polarised laser field. Subsequently, in 2024, this developed wave function was employed to investigate the DCS in a linearly polarised laser field. Building upon these advancements, this study aims to explore the DCS utilizing the thermal wave function and thermal Coulomb potential. The wave function adopted from Dhobi *et al.* is paired with the thermal Coulomb potential, as proposed by Solovyev *et al.*, comprehensively examine the thermal aspects of scattering dynamics [5]. Dhobi *et al.* developed a mathematical model to investigate the interaction between the Hamiltonian containing quantum entities near the PEMFC electrode as well as the PEMFC output., focusing on the DCS and current in a thermal environment [6]. To achieve the desired voltage, PEMFCs rated close to 0.7 V are arranged in series and parallel combinations. While previous studies have focused on the system Hamiltonian, defined as the sum of the total energy of sub-components with their interactions [7], our proposed Hamiltonian is specifically the sum of the potential and kinetic energy of quantum species formed around the electrode of the system.

Energy is one amongst the most significant forces driving the world economy. Despite ongoing study and investigation into other energy sources, fossil fuels remain dominant. There are various harmful environmental impacts associated with fossil fuels. To remove the negative effect impact on the environment by fossil fuel one of the best alternative renewable energies is hydrogen. To convert hydrogen into energy a device fuel cell is one of the most demanding green technologies with a variety of uses, that range from a small tiny gadget to a large one [8]. A lot of investigation is being done to improve performance, endurance, efficiency in costs, and eliminate the limitations of fuel cells. Japan's New Energy as well as Industrial Technology Development Organisation is aiming for short and long-term power density targets of 6 kilowatts per liter by 2030 and 9 kilowatts per liter by 2040 [9-10]. Japan plans to manufacture 200,000 automobile FCEVs by 2025, the United Kingdom aims to manufacture a large number of FCEVs (cars, trucks, and buses), while China aims to produce one million FCEVs until 2030. The hydrogen fuel cell industry has expanded quickly in the past few years, with around 70,000 systems using fuel cells producing approximately USD 2.3 billion annual revenue. More than 300,000 standalone fuel cells are in operation worldwide, including 14,000 hydrogen-powered fuel-cell vehicles on the road and approximately 300 hydrogen-refueling stations by 2050 [11].

Optimization of bipolar plate flow channels to enhance mass transfer and water removal, where a contraction ratio of 0.25 and specific channel designs improve PEMFC performance under certain conditions [12]. The impact of elevated temperatures (80-95°C) on PEMFC performance, indicating increased ohmic loss, reduced ECSA, and the influence of humidity on current density [13]. Flow field design for improving water-gas transport characteristics, emphasizing the need for cost-effective commercial flow field plates [14]. Advances in small-scale PEMFC applications, focusing on portable and stationary power solutions [15]. Detailed analysis of membrane and bipolar plate materials and their production methods [16]. However, no studies were found that investigate the relationship between DCS and PEMFC parameters such as current and voltage, leaving this an unexplored area.

To improve the efficiency of PEMFCs, optimizing the interactions between electrons, protons, and hydrogen molecules around the electrodes is crucial. While various factors affect PEMFCs performance, this work focuses on the interactions between quantum species (electron, proton, and hydrogen) around the electrode in a photonic field, with different IR frequencies generated during the reaction. The study aims to investigate the scattering effects and energy losses associated with electron-proton collisions, as these interactions are critical for current and voltage generation in PEMFCs. The interaction time and region of quantum species determine the flow rate of electrons, known as current. Delays in these interactions can reduce electron flow, thereby decreasing current production. Additionally, the contact region influences the delay that occurs during electron flow. As a result, the goal of this study is to better understand the area of interaction known as DCS when there is the presence of an external laser field. By addressing these factors, the overall efficiency and performance of PEFCs can be substantially enhanced. This work seeks to bridge the theoretical understanding of scattering with practical green technology applications, representing its novel contribution.

1.1 Problem of Statement/Research Gap

In 2022, Dhobi *et al*. studied the interaction between free electrons and ions, and their effect on output current of a PEMFC, considering the cause-and-effect assumption and found relationship wherein current is produced by quantum species around the electrode. However, they were unable to link the interaction region DCS of these quantum species with the current produced in the PEMFC. Understanding this interlink between DCS and current is crucial, as it helps determine the optimal region around the electrode necessary for maximizing current, output power and the effectiveness of the PEMFC. The power and efficiency are directly related to current production during quantum species flow in a thermal environment, created by the exothermic reaction between H_2 and Pt. This reaction provides IR thermal radiation (1.7 eV to 1.24 mV), acting as a laser-assisted scattering system initiated by the Volkov wave function and derived using the Kroll-Watson and Byron-Joachain approximations. This work aims to develop a theoretical model for the interaction region (DCS) around the electrode of a PEMFC and its relationship with the output current, aiming to improve the efficacy and power of PEMFC.

1.2 Significance of Research Work

The interconnection of the DCS with the current in a PEMFC significantly impacts the study of its efficiency. Based on this model, researchers can design experiments to improve PEMFC efficiency, reduce temperature impact, and enhance overall performance. Understanding the interaction region helps determine the optimal fuel flow density, as not all input hydrogen participates in the quantum species formation during the H_2+Pt reaction. Some hydrogen remains unused and is recycled, increasing system complexity. By determining the interaction region (DCS), we can control the fuel rate, maximize current extraction, and improve the efficiency and power output of PEMFC.

1.3 Research Gap

While previous studies have extensively explored the DCS and PEMFC separately, there is a notable gap in research interlinking DCS with various parameters of PEMFC, specifically current and voltage, around the electrode region. No prior work has investigated how these factors interact in the localized thermal environment generated by the exothermic reaction between hydrogen and the electrode catalyst, along with collisions between electrons, protons, and hydrogen molecules. Additionally, while studies have referenced thermal conditions in PEMFC, there has been no experimental analysis combining the behavior of electrons, protons, and hydrogen in the thermal environment, which acts as a weak laser source, with temperature ranges from room temperature to 120°C. This integration of DCS and PEMFC under such thermal conditions remains unexplored and represents a significant opportunity for advancing the understanding of fuel cell dynamics.

2. METHOD AND MATERIALS

The dynamics system associated with an unbound electron within a developed laser field receive little attention in the literature, despite their importance in many domains of nuclear as well as general physics. Regardless of the gauge, the following Hamiltonian can explain a single atom electron structure that includes a light field with the vector potential ($\vec{A}(\vec{r},t)$) and an electric field with the scalar potential (φ) [1]:

$$H = \frac{\vec{p}^2}{2} - \frac{1}{2}\left(\vec{A}(\vec{r},t).\vec{p} + \vec{p}.\vec{A}(\vec{r},t)\right) + \frac{\vec{A}^2(\vec{r},t)}{2} - \varphi + \frac{3}{2}k_B T \qquad (1)$$

But for our system we have consider quantum species the Hamiltonian is consider as

$$H = \sum\left(\frac{\vec{p}^2}{2} - \frac{1}{2}\left(\vec{A}(\vec{r},t).\vec{p} + \vec{p}.\vec{A}(\vec{r},t)\right) + \frac{\vec{A}^2(\vec{r},t)}{2} - \varphi + \frac{3}{2}k_B T\right) \qquad (2)$$

where A is vector potential and p is momentum. The scalar potential of a hydrogen-like atom having charge Z is: $\varphi = \left(\frac{4\zeta(3)}{3\pi\beta^3}r^2 - \frac{4\zeta(5)}{5\pi\beta^5}r^4\right)$ [5]. The time-dependent Schrödinger equation (TDSE) that describes the atomic single electron system reads:

$$i\hbar\frac{\partial}{\partial t}X(\vec{r},t) = HX(\vec{r},t) \qquad (3)$$

Beyond the dipole approximation, the most famous gauges within strong-field physics are the Lorentz and Coulomb gauges [17].

$$X(r,t) = \frac{1}{(2\pi)^{3/2}}exp\left\{i\frac{p}{\hbar}.\left(r + \frac{e}{m}\int A(t')dt'\right) - i\frac{E}{\hbar}t - i\frac{e^2}{2m\hbar}\int A^2(t')\right\}dt' \qquad (4)$$

Volkov wave function for linear polarized $\boldsymbol{A} = \boldsymbol{a}cos(\omega t)$ where $a = A_0 = \sqrt{\frac{8\pi\mathcal{N}_\omega\hbar}{\omega\mathcal{V}}}$, is vector potential amplitude, consider a volume $\mathcal{V}$ with a number of photons N_ω the energy density. Now from Equation (4) the linear Volkov wave function for thermal case [18] is obtained as:

$$X_{TL}(r,t) = \frac{1}{(2\pi)^{3/2}}exp\left\{i\frac{p}{\hbar}.\left(r + \frac{e}{m}\frac{a}{\omega}\sin(\omega t)\right) - \frac{i}{\hbar}\left(E + \frac{a^2e^2}{4m}\right)t - i\frac{e^2a^2\sin(2\omega t)}{8m\hbar\omega}\right\} - k_e\nabla T_{eiT}\exp(i\omega_{eiT}t) \qquad (5)$$

This is the wave function that will be used to explain electrons in a laser field. The solution for Equation (3) can be discovered in the atomic physics textbooks by B. H. Bransden and C. J. Joachain. Where $k_e\nabla T_e\exp(i\omega t)$ thermal the wave function (k_e is electrons the thermal conductivity), variation in the temperature of electron [19]. For elliptical the modified

Volkov wave function for thermal electron is obtained using vector potential $A = \boldsymbol{a}\left[\hat{x}\cos(\omega t) + \hat{y}\sin(\omega t)\tan\left(\frac{\eta}{2}\right)\right]$ and for circular polarized $\eta = \frac{\pi}{2}$ and for linear $\eta = 0$. The scattering angle γ is defined as $\tan^{-1}\left\{\tan\theta \,.\, \tan\left(\frac{\eta}{2}\right)\right\}$.

2.1 Current Production from PEMFC due Quantum Species

In the system of a PEMFC, the inlet hydrogen produces electrons and protons, along with residual hydrogen and heat energy. This heat energy creates a system involving electrons, protons, and a laser field, where the laser field refers to the IR energy produced during the reaction. The interaction of these electrons, protons, and residual hydrogen is crucial for generating electric current in the PEMFC, which determines its efficiency. The Butler-Volmer equation defines the voltage and current outputs of a PEMFC, which is one of the most important relationships within electrochemical kinetics. This equation explains the way the current flowing on an electrode relates to the electrode potential [20],

$$I = A.i_0\left\{\exp\left[\frac{\beta_a n_e F}{RT}\left(E - E_{eq}\right)\right] - \exp\left[-\frac{\beta_c n_e F}{RT}\left(E - E_{eq}\right)\right]\right\} \quad (6)$$

Solving for T from Equation (6) we get, $T_{cell} = \frac{n_e F(E - E_{eq})}{R\log\left(\frac{I}{Ai_0(e^{\beta a} - e^{\beta c})}\right)}$, Here T is temperature which vary with reaction also known as cell temperature, I is current across load, i_0 is the exchange current density, E is the electrode potential, and E_{eq} is the equilibrium potential. T is the absolute temperature, n_e is the number of electrons participating in the electrode reaction, F is the Faraday constant, R is the universal gas constant, and β_c is the dimensionless cathodic as well as β_a is the anodic charge transfer coefficient, η is the activation overpotential ($\eta = \left(E - E_{eq}\right)$) and the value is $\beta_a + \beta_c = 1$, $\beta_a \approx \beta_c \approx \beta = 0.5$.

2.2 DCS with Polarization

We choose a derivation akin to that demonstrated by Kroll and Watson in 1973 and from relation of scattering matrix transition matrix we have transition matrix for linear polarized for different Bessel using DCS from [21] we have:

$$\frac{d\sigma^L}{d\Omega} = \frac{p_{efT}}{p_{eiT}}\left|\left\{J_n\left(-\frac{e}{\hbar m\omega}\boldsymbol{q}.\boldsymbol{a}\right)f^1_{Born} - k_e T_{cell}\frac{\delta\left(\omega_{efT} - \omega_{eiT}\right)}{\delta\left(E_{efT} - E_{eiT} + n\hbar\omega\right)}\right\}\right|^2 \quad (7)$$

The first term of the formula (7) is the same as derived from Kim in 2022 in his doctoral dissertation [21], while the following one is innovative and does not arise at the date since the authors disregard the thermal scattering caused by electrons in laser fields, assume that $\nabla T_{eiT} + \nabla T_{efT}$ as absolute temperature of cell as T_{cell} is obtained from Equation (6). Using relation $\delta\left(E_{fT} - E_{iT} \pm n\hbar\omega\right) = \delta(E_{fT} - E_{iT})\delta(E_{fT} \pm n\hbar\omega)$ [22] for n photon. Where $f_{Born}{}^{(1)}$ of Equation (7) is born first approximate obtained by Fourier transformation obtained as,

$$f_{Born}{}^{(1)} = -\frac{4\pi}{q}\left[-\frac{4\zeta(3)}{3\pi\beta^3}\left(\frac{e^{iqr}(-iq^3r^3 + 3q^2 + 6iqr - 6)}{q^4} + \frac{e^{-iqr}(iq^3r^3 + 3q^2 - 6iqr - 6)}{q^4}\right) - \frac{4\zeta(5)}{5\pi\beta^5}\left(\frac{e^{-iqr}(iq^5r^5 + 5q^4r^4 - 20iq^3r^3 - 60q^2r^2 + 120iqr + 120}{q^6} + \frac{e^{iqr}(-iq^5r^5 + 5q^4r^4 + 20iq^3r^3 - 60q^2r^2 - 120iqr + 120)}{q^6}\right)\right] \quad (8)$$

Similar as DCS obtained for linear polarization in thermal environment, DCS for elliptical polarized with thermal electron obtained as:

$$\frac{d\sigma}{d\Omega} = \frac{p_{efT}}{p_{eiT}}\left|J_n(R\cos\gamma)f^1_{Born} + k_e T_{cell}\frac{\delta\left(\omega_{efT} - \omega_{eiT}\right)}{\delta\left(E_{efT} - E_{eiT} + n\hbar\omega\right)}\right|^2 \quad (9)$$

Where $R = \frac{iea}{m\omega c}$ and assume that $\nabla T_{eiT} + \nabla T_{efT}$ is equivalent to absolute temperature of system. Also, the DCS for circular polarized with thermal electron using applying Kroll Watson approximation and scattering-transition matrix is obtained as:

$$\frac{d\sigma}{d\Omega} = \frac{p_{efT}}{p_{eiT}}\left|J_n(R\cos\beta)f^1_{Born} + k_e T_{cell}\frac{\delta\left(\omega_{efT} - \omega_{eiT}\right)}{\delta\left(E_{efT} - E_{eiT} + n\hbar\omega\right)}\right|^2 \quad (10)$$

3. RESULT AND DISCUSSION

The developed theory, as described by Equations (7), (9), and (10), was computed to investigate the behavior of the DCS under various parameters, including the scattering angle, incident energy of electrons, and separation distance between the target and incident electron, both in the absence and presence of temperature effects. The simulations encompassed a wide range of conditions: scattering angles ranging from 0 to 360°, incident electron energies spanning from 0 to 20 MeV (but for this work we are interest in 0 to 0.511MeV because the energy of electron after formation from H_2 approximate 0.511MeV and it get reduce due to interaction), and Bessel function orders ranging from 1 to 3. Furthermore, for scenarios involving linear polarization, the simulations considered scattering angles from 0 to 360° and separation distances between the electron and target ranging from 0 to 40 nanometers. These comprehensive simulations enabled a detailed exploration of the DCS across various parameter spaces, shedding light on its behavior under different experimental conditions.

3.1 DCS for Linear Polarization Laser Field

The DCS exhibits a distinct trend with respect to the scattering angle, as observed in Figure 1 for linear polarized laser field interactions with thermal electrons and thermal potential of hydrogen atoms. This thermal

environment is self-created with H_2 touch the electrode of which is coated with Pt in PEMFC system. Initially, the DCS sharply decreases as the scattering angle increases from 0 to 90º, followed by an increase reaching a maximum around 150º. Subsequently, the DCS decreases sharply again, reaching a minimum beyond 250º. This behavior is in accordance with Equation (7), which governs the nature of the DCS in the studied scenario. It is observed that at lower scattering angles (below 90º) and beyond 250º, the DCS is higher. However, between the angles of 90º to 250º, the trend is reversed, with the DCS of lower temperatures being higher than that of higher temperatures. This reversal in the nature of the DCS with varying scattering angles is consistent with findings by [23] for different screening parameters and incident energy cases involving Li, K, and Na. Specifically, they observed that the DCS is higher at smaller scattering angles (below 40º) for certain incident energy cases, but decreases with increasing scattering angle beyond 40º. Such a nature of the DCS is also evident in the present study for thermal cases.

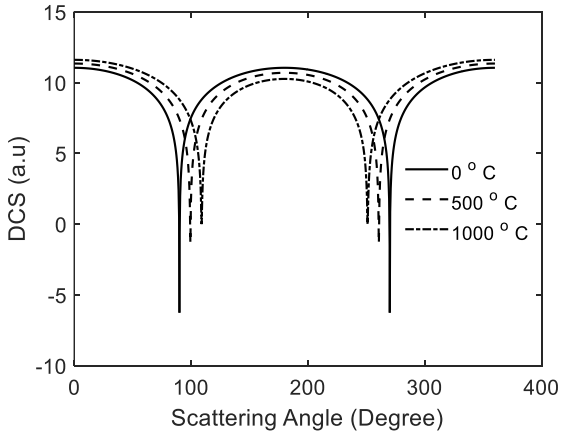

Fig. 1. Linear polarization with scattering angle.

Comparing with the findings of Harris *et al*. for linear polarized laser field interactions with electron-hydrogen scattering, it is noted that while both studies exhibit a similar trend of the DCS, there are differences in the details [24]. Specifically, while the present study shows a flat nature of the DCS, Harris *et al*. obtained a Bessel-type decay nature initially, followed by a reverse trend with further increasing scattering angles after a certain threshold. These observations highlight the complex and new nature of the DCS in electron-atom scattering processes under various conditions, shedding light on the underlying physics governing such interactions.

The observed peaks and troughs in the DCS can be attributed to the phenomenon of interference between the laser field and the free or projected electron. Destructive interference leads to the formation of troughs, while constructive interference results in peaks. This behavior arises from the superposition principle, where the influence of the target and its surroundings contributes to the DCS pattern. Specifically, at lower incidence energies, the DCS is higher due to resonance effects induced by the incident electron interacting with the target. This resonance occurs over a longer time period within a smaller energy range, leading to pronounced peaks. Conversely, at higher incidence energies, the probability of electron-target interaction decreases, resulting in a predominance of oscillatory patterns in the DCS, as depicted in Figure 2. The resonance phenomenon primarily occurs near the fixed target, as the distance between the projected electron and the target remains constant throughout the study. However, the energy of the projected electron varies, influencing the resonance characteristics.

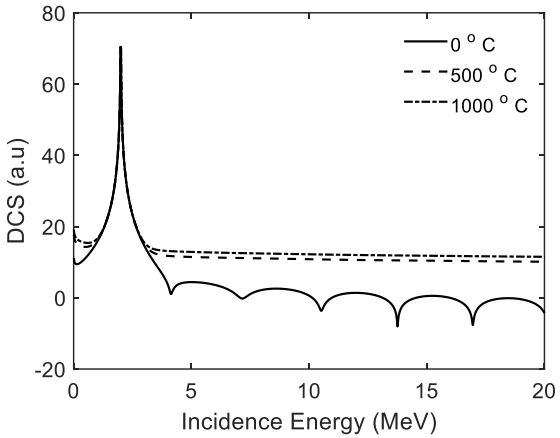

Fig. 2. Linear polarization with incidence energy.

Figure 2 depicts the DCS variation with incidence energy, revealing intriguing patterns. This suggests that temperature dominates the damping effect of the Bessel function at higher energies. Furthermore, the DCS for lower energy cases across different orders of the Bessel function, demonstrating that lower orders correspond to higher energies, and vice versa. However, in the higher energy region (>5 MeV), the DCS for higher order Bessel functions surpasses that of lower order functions, indicating a reversal in the trend. The observed trends in the DCS findings are consistent with previous research [25], which investigated linear polarized laser field interactions with electron-Kr scattering. A similar pattern was observed for elliptical and circular polarizations, with the DCS being higher than that of linear polarization. Furthermore, the DCS of elliptical polarization was higher than that of circular polarization. In general, the DCS for elliptical polarization was the highest, followed by circular, and then linear. Additionally, the DCS for the first order of the Bessel function was higher than for other orders.

The DCS analysis with varying distance separation between the target (residual hydrogen) and the projected electron (formed electrode with Pt+H_2 reaction), as illustrated in Figure 3 around electrode of PEMFC, sheds light on the intricate interplay between these parameters. Equation (6) serves as the theoretical foundation for understanding the DCS behavior concerning electron energy and distance separation inside PEMFCs around electrode of PEMFC. The observed trend indicates that the DCS increases with

distance separation, a phenomenon attributed to the widening separation between the projected electron and the target. This increased separation enhances the probability of electron-photon interaction over a larger spatial region, consequently leading to an elevated DCS.

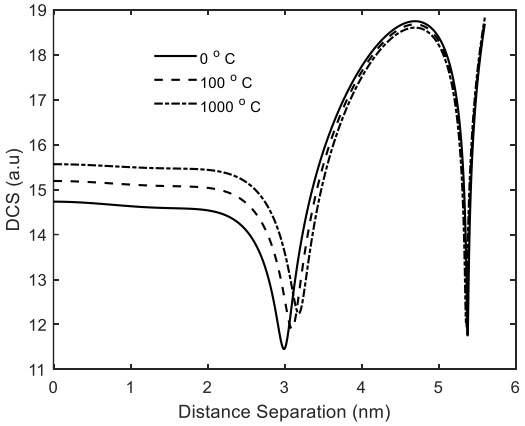

Fig. 3. Linear polarization with distance.

The constructive and destructive interference effects become more pronounced with increasing distance separation between the target and the electron in the laser field. This is because, for a fixed incidence angle, the target's influence is more significant when the electron spends more time in close proximity to the target. Conversely, at shorter distances, the interaction phenomena are attenuated due to reduced interaction time, resulting in lower DCS values. Furthermore, the DCS variation with distance separation at different temperatures. The observations reveal that higher temperatures of thermal electrons and thermal potentials correspond to higher DCS values, particularly for separation distances up to 3 nm. Beyond this threshold, the DCS begins to decrease, indicating a transition towards destructive interference effects dominating over constructive ones. Interestingly, the temperature effect remains prominent until approximately 4.5 nm separation distance, beyond which its influence diminishes, consistent with the onset of destructive interference. A similar pattern was observed for elliptical polarization based on Equation (9) and circular polarization based on Equation (10), with the DCS being higher than that of linear polarization. Additionally, the DCS for elliptical polarization was higher than that of circular polarisation. In general, the DCS was highest for elliptical polarization, followed by circular, and then linear.

The investigation into the DCS concerning scattering angle in the elliptical case unveils a nuanced behavior characterized by a decrease in DCS at very small scattering angles. This intriguing observation, depicted in Figure 4, can be attributed to the inherent properties of the Bessel function, particularly within the narrow region between 1.55° to 1.60°, as elucidated by Equation (9). The oscillatory nature of the Bessel function gives rise to constructive and destructive interference phenomena, resulting in a gradual decline in DCS with increasing scattering angle. Notably, the DCS associated with the first-order Bessel function surpasses that of higher orders, underscoring the dominance of interference effects.

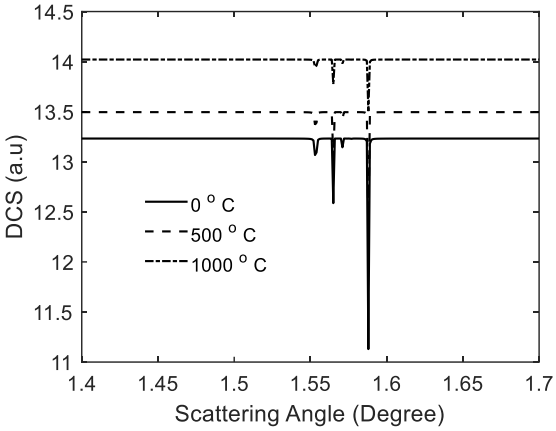

Fig. 4. Elliptical polarization with scattering angle.

Moreover, the influence of temperature on DCS at varying scattering angles. The observations reveal a direct correlation between temperature and DCS, with higher temperatures yielding elevated DCS values, particularly for the first-order Bessel function. This temperature-dependent behavior can be elucidated through Equation (9), where temperature directly influences the interaction dynamics between atoms and electrons, leading to atom expansion and subsequent enhancement of DCS with increasing temperature. The distinctive features observed in the DCS plots, such as the downward peaks indicative of destructive interference and the straight lines representing the superposition of waves with equal amplitude, underscore the intricate interplay between interference effects and scattering phenomena. The DCS for elliptical polarization was greater than for circular polarization, and the DCS for circular polarization was greater than for linear polarization, as a function of the scattering angle. Elliptical and circular polarizations exhibited constructive and destructive interference predominantly in the lower scattering angle region, whereas linear polarization showed minimal interference, primarily at higher scattering angles.

The study of DCS with parameters such as scattering angle, momentum, and distance separation demonstrates how the interaction region around the electrode fluctuates in a thermal environment (Figure 1 to Figure 4). This analysis is crucial for determining the optimal conditions for enhancing the efficiency of PEMFC, as referenced in sources (10) and (6). In terms of the screening effect, a lower DCS is more favorable. Lower DCS values indicate reduced screening, which allows electrons to move more freely within the system. This lower screening effect means that fewer electrons are blocked or diverted, enabling more electrons to participate in the current generation process. As a result, the overall efficiency of the PEMFC is increased, since a higher flow of electrons through the circuit enhances current production.

On the other hand, when focusing on interaction dynamics, a higher DCS is preferred. High DCS values suggest a stronger likelihood of electron-proton and molecule-molecule interactions. This increased interaction facilitates better electron generation, contributing to a more efficient current flow. However, with higher DCS, the probability of electron screening also increases. While high DCS supports greater interaction, the dominant screening effect might resist the flow of electrons, creating a trade-off between interaction and screening. Thus, while higher DCS promotes electron generation, excessive screening may limit the flow of electrons, impacting the fuel cell's efficiency. Therefore, balancing the DCS is essential to optimize both the electron interaction and screening processes, ultimately improving the overall performance of PEMFCs.

3.2 DCS and Current Production of PEMFC

Considering Equation (7), which is linked to the temperature generated within the fuel cell around the electrode, and Equation (6) of the PEMFC current, it is observed that when electrons are generated, thermal energy is also generated, akin to laser-assisted scattering. In this research, two activation potentials of Pt/C (40 mV and 55 mV), two electrons (H_2) to many electrons (H_2), with anodic and cathodic charge transfer coefficients summing to 1, F as the Faraday constant, R as the universal gas constant, and i_0 as the exchange current density are considered. Figure 5 illustrates the impact of the resultant output current generated by PEMF due to quantum species formed around the electrode of the PEMFC. Figure 5(a) represents a single hydrogen flow as input, while Figure 5(b) shows the effect of 100 hydrogen flow as input gas. Both figures depict that the DCS increases with the resultant current increase. The DCS for a single hydrogen flow is observed to be generated and widely varied compared to 200 electrons. Initially, for 200 electrons, the DCS decreases with resultant current production due to destructive interference between quantum species and screening effects between quantum species formed due to inlet fuel. However, with increasing resultant output current, the DCS increases due to superposition and increasing flow rate with Coulomb repulsion. A similar trend is observed for Pt/C 55 mV, but the DCS is slightly higher (about 0.2 a.u.) than for 40 mV, considering other parameters constant.

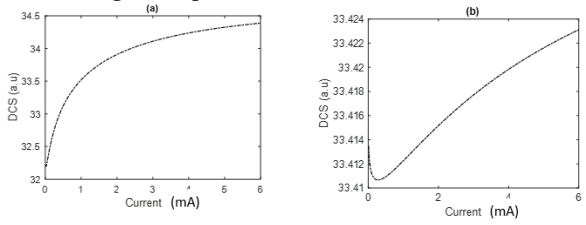

Fig. 5. Impact of resultant output current on DCS among quantum species produce by (a) 1 cm^2 and (b) 5 cm^2 with flow of one H_2 per millsec and 100 H_2 per millisec for activation potential Pt/C 40mV.

Figure 6 illustrates the impact of interaction surface size on hydrogen production, with 200 and 2000 electrons respectively generated by hydrogen when interacting with the Pt electrode. In Figure 6(a) and (b), it is evident that the DCS increases with the resultant output current of the PEMFC. This indicates that the interaction region expands with increasing current and the number of electrons formed during the H2/Pt reaction. However, it's noteworthy that while the interaction region increases with 2000 electrons, the DCS remains constant. This suggests that the DCS does not increase with current because the dimension of the electrode is fixed, and the density of quantum species is also fixed. The higher interaction region observed with 2000 electrons can be attributed to screening effects between quantum species, which enhance the interaction region despite the fixed electrode dimensions.

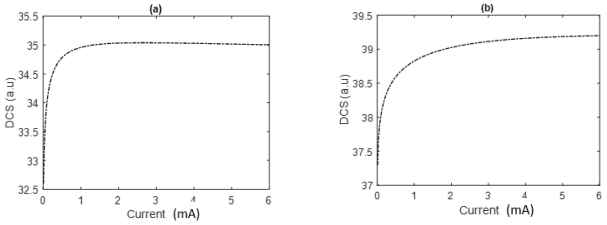

Fig. 6. Impact of resultant output current on DCS among quantum species produce by (a) 1 cm^2 and (b) 5 cm^2 with flow of one H_2 per millsec and 100 H_2 per millisec for activation potential Pt/C 55 mV.

In Figure 7, the relationship between charge and the DCS for different surface areas is depicted. In Figure 7(a), for smaller surface areas, a linear relation is observed, indicating a proportional increase in DCS with the charge. However, in Figure 7(b), for larger surface areas, a different trend is noticed. Initially, the DCS decreases and then gradually increases with the charge. This observed increase in DCS can be attributed to the screening effect of electrons around the electrode. The screening effect influences the flow of electrons, which is directly related to the current. Therefore, any barriers in the flow of current decrease the DCS, while facilitating the flow of electrons leads to an increase in the DCS of interacting particles.

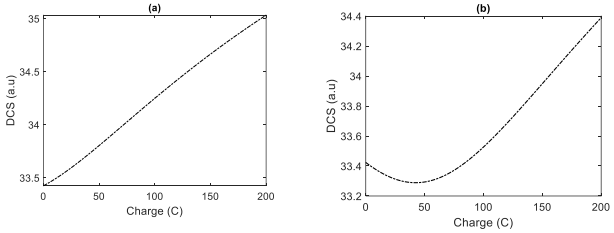

Fig. 7. Impact of charge production on DCS among quantum species produce by (a) 1 cm^2 and (b) 5 cm^2.

In Figure 8(a), the DCS decreases with the exchange current density of the electrode of surface area. Similar results were observed for a Pt/C activation potential of 55 mV, as depicted in Figure 8(b), although at a higher level compared to the 40 mV scenario. Initially, the DCS increases and reaches a maximum due to constructive interference, indicating a higher

probability of interaction, as shown in Figure 8(a). However, the subsequent decrease in DCS is attributed to the interference of formed quantum species and the charge on the surface of the electrode, leading to a screening effect and consequently reducing the DCS. Figure 8(b) demonstrates a decrease in DCS exponentially with a surface area of 5 cm^2. Unlike in the case of smaller surface areas, no peak is observed here, indicating the absence of interference. Instead, a superposition of effects, along with reduced screening effects, is evident. With a larger electrode area, the distribution of quantum species is more uniform, resulting in a non-linear decay in DCS due to the diminished screening effect.

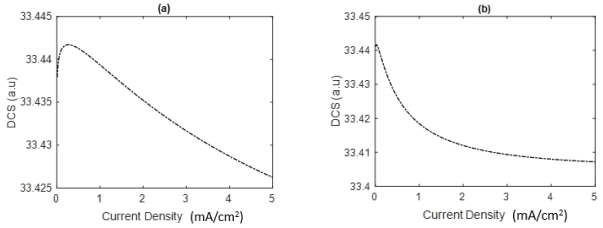

Fig. 8. Impact of electrode current density on DCS among quantum species produce by (a) 1 cm^2 and (b) 5 cm^2 with flow of one H_2 per millsec and 100 H_2 per millisec.

3.3 Temperature and Current Density

Figure 9 illustrates the impact of current density on the temperature of PEMFC, revealing a notable trend: as current density increases, the temperature of PEMFC decreases. This observation may seem counterintuitive at first glance. However, it can be explained by the dynamics within the system. With a larger number of quantum species, collisions and reactions occur more frequently, leading to higher temperatures. Conversely, as current density increases, the temperature decreases for a fixed surface area. This phenomenon occurs because initially, after the formation of quantum species, the temperature is higher due to exothermic reasons. However, as electrons become liberated from hydrogen molecules, the density decreases, resulting in shorter collision paths and lower kinetic energy. Consequently, collisions produce lower temperatures, causing the overall system temperature to decrease. It's worth noting that negative temperatures may exist, but for the purposes of this discussion, we focus solely on positive temperature regions.

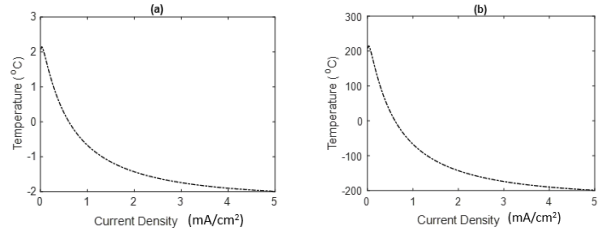

Fig. 9. Impact of charge production on DCS among quantum species produce by (a) 1 cm^2 and (b) 5 cm^2.

Figure 10 depicts the relationship between temperature and resultant output current density, revealing distinct patterns for different surface areas. In Figure 10(a), for smaller surface areas, the temperature exhibits an exponential increase with increasing current density until reaching a certain threshold, beyond which it begins to decrease. This behavior can be attributed to the dynamics within a confined space: initially, collisions are reduced, leading to lower kinetic energy and subsequently lower temperature. However, at lower currents, the dominant factor is the heat generated by exothermic reactions, causing the temperature to increase. Conversely, in Figure 10(b), for larger surface areas, the temperature continues to increase with current density. Here, collisions contribute additional thermal energy to the exothermic energy, leading to a continuous rise in temperature. This difference in behavior underscores the significance of surface area in influencing the thermal dynamics within the PEMFC system.

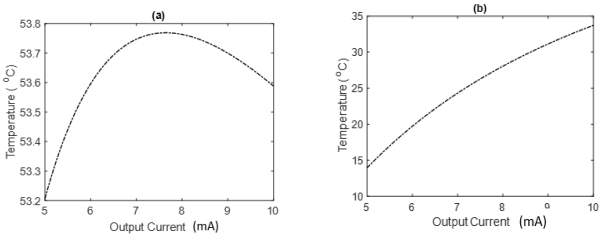

Fig. 10. Resultant output current and termapture realtion with surface (a) 1 cm^2 and (b) 5 cm^2.

Figure 11 illustrates a noteworthy trend wherein temperature decreases with increasing surface area for varying numbers of electrons generated by the inlet of H_2. This phenomenon arises due to the interplay between electron density, quantum species distribution, and collision dynamics within the fixed surface area. Specifically, when the surface area is fixed and the number of electrons increases, the density of quantum species also rises, leading to a corresponding increase in collision frequency. Consequently, at a specific surface area, varying electron densities result in different temperatures. For instance, in Figure 11(a) and Figure 11(b), observed at approximately 1cm^2, the temperature varies due to the differing collision rates and heat contributions to exothermic reactions. This finding underscores the critical role of surface area in modulating collision dynamics and subsequent thermal behavior within the PEMFC system.

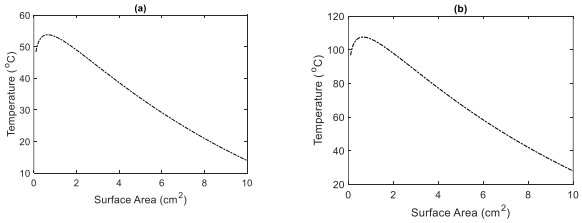

Fig. 11. Effect of surface area on temperature of PEMFC with (a) n=50, (b) n=100.

Figures 5 through 11 illustrate the impact of various PEMFC parameters on DCS. By analyzing these effects, we can optimize the efficiency of PEMFC and gain a deeper understanding of the reciprocal relationship between PEMFC parameters and DCS. The

figures clearly demonstrate how parameters such as current, voltage, scattering angle, momentum, and distance separation influence DCS, and how, in turn, DCS affects these parameters. The observations reveal that all these parameters are interrelated, with each playing a significant role in altering DCS behavior. This relationship provides valuable insights into the underlying mechanisms governing electron flow, proton-electron interactions, and overall fuel cell performance. By understanding how these variables interact, it is possible to optimize conditions that enhance PEMFC efficiency, ensuring better current generation and reduced energy losses.

3.4 Future Work

The interconnection of DCS and PEMFC will provide valuable insights into the interaction region around the electrode and how temperature influences DCS and hydrogen polarization. This study will also examine the screening effect on electron flow and the interactions between electrons and protons through Coulomb forces, as well as interactions among molecules (electron-molecule, proton-molecule, and molecule-molecule) within a thermal environment. These interactions are crucial in screening the electrons involved in current generation within the fuel cell, ultimately impacting the overall current production.

4. CONCLUSION

This study developed the complex dynamics of the DCS within PEMFC, elucidating the interactions of quantum species within thermal environments created during H_2/Pt reactions. Through extensive simulations, we analyze the behavior of DCS under various parameters, including scattering angles, incident electron energies, and particle separation distances, accounting for temperature effects. Findings unveil subtle patterns in DCS across different conditions, with significant implications for enhancing PEMFC efficiency and performance. Specifically, observations of DCS across different polarization states provide insights into quantum species behavior and its influence on PEMFC operation. Furthermore, exploration of the relationship between DCS and PEMFC current production offers valuable insights for optimizing power generation within PEMFC. Additionally, analyses of interaction surface size, charge, and electrode current density contribute to a deeper understanding of DCS behavior, guiding strategies for enhancing PEMFC performance. Moreover, investigation into temperature variations within PEMFC highlights the importance of thermal management strategies in PEMFC design, especially concerning current density and surface area considerations.

ACKNOWLEDGEMENT

I would like to express my heartfelt gratitude to all faculty members of the Central Department of Physics, Tribhuvan University, Kritipur, Kathmandu, and the Department of Physics, Patan Multiple Campus, Tribhuvan University, Patandhoka, Lalitpur, Nepal, for their invaluable guidance and support. I am grateful to the team members of ICETIGT-2024 for their collaborative efforts. Lastly, I would like to acknowledge the University Grants Commission (UGC) of Nepal for providing the grant that made this research possible.

REFERENCES

[1] Dhobi, S. H., Nakarmi, J. J., Yadav, K., Gupta, S. P., Koirala, B., and Shah, A. K. (2022). Study of thermodynamics of a thermal electron in scattering. Heliyon, 8(195602), e12315. https://doi.org/10.1016/j.heliyon.

[2] Banerji, J., and Mittleman, M. H. (1995). Electron-hydrogen atom scattering in a super-intense laser field. Journal of Physics B: Atomic, Molecular and Optical Physics, 28(16), 3603–3614. https://doi.org/10.1088/0953-4075/28/16/013

[3] Bhattacharya, M., Malakar, B., and Sarkar, S. (2002). Scattering of Electron by Hydrogen Atom in the Presence of Two Laser Fields. Physica Scripta, 66(3), 208–212. https://doi.org/10.1238/physica.regular

[4] Dahiri, I., Baouahi, M., Ouali, M., Manaut, B., El Idrissi, M., and Taj, S. (2023). Laser-assisted electron–nucleon scattering. International Journal of Modern Physics B. https://doi.org/10.1142/S0217979224502898

[5] Solovyev, D., Zalialiutdinov, T., and Anikin, A. (2021). Relativistic corrections to the thermal interaction of bound particles. Physical Review Research, 3, 023102. https://doi.org/10.1103/PhysRevRes.3.023102

[6] Dhobi, S. H., Yadav, K., Jha, A. K., Karki, B., and Nakarmi, J. J. (2022). Free Electron-Ion Interaction and Its Effect on Output Current of Permeable Exchange Membrane Hydrogen Fuel. ECS Transactions, 107, 8457. DOI: 10.1149/10701.8457ecst

[7] Li, Y., Cheng, B., Zhang, K., Li, X., Pang, S., and Mao, Z. (2023). Adaptive Hamiltonian-Based Energy Control with Built-In Integrator for PEMFC Hybrid Power Conversion Architecture. Energies, 16, 7855. https://doi.org/10.3390/en16237855

[8] Alaswad, A.,. Omran, A., Sodre, J.R., Wilberforce, T., Pignatelli, G., Dassisti, M., Baroutaji, A., Olabi, A.G. Energies, 14(144), (2021).

[9] Jiao, K., Xuan, J., Du, Q., Bao, Z., Xie, B., Wang, B., Zhao, Y., Fan, L., Wang, H., Hou, Z., Huo, S., Brandon, N.P., Yin, Y., and Guiver, M.D. Nature, 595, (2021).

[10] Habib, MD. S., Arefin, P., Salam, MD. A., Ahmed, K., Uddin, MD. S., Hossain, T., Papri, N., Islam, T. Mater. Sci. Res India, 18(2), (2021).

[11] Tellez-Cruz, M.M., Escorihuela, J., Solorza-Feria, O., Compañ, V. Polymers, 13(3064), (2021).

[12] Yin, T., Chen, D., Hu, T., Hu, S., Li, Y., and Xu, X. (2024a). Optimization of variable cross-sectional flow channel parameters for fuel cells: Numerical analysis and distributional uniformity evaluation. Applied Thermal Engineering, 243, 122639.

[13] Yin, T., Chen, D., Hu, T., Hu, S., Li, R., Wei, T., and Pei, P. (2024b). Experimental investigation and comprehensive analysis of performance and membrane electrode assembly parameters for proton exchange membrane fuel cell at high operating temperature. Energy Conversion and Management, 315, 118740.

[14] Zhou, Y., and Chen, B. (2023). Investigation of optimization and evaluation criteria for flow field in proton exchange membrane fuel cell: A critical review. Renewable and Sustainable Energy Reviews, 185, 113584.

[15] Wang, Z., Liu, Z., Fan, L., Du, Q., and Jiao, K. (2023). Application progress of small-scale proton exchange membrane fuel cell. Energy Reviews, 2(2), 100017.

[16] Kahraman, H., and Akın, Y. (2024). Recent studies on proton exchange membrane fuel cell components, review of the literature. Energy Conversion and Management, 304, 118244.

[17] Maurer, J., and Keller, U. (2021). Ionization in intense laser fields beyond the electric dipole approximation: concepts, methods, achievements and future directions. Journal of Physics B: Atomic, Molecular and Optical Physics, 54(9), 094001. https://iopscience.iop.org/article/10.1088/1361-6455/abf731/pdf

[18] Dhobi, S. H., Gupta, S. P., Yadav, K., Nakarmi, J. J., and Jha, A. K. (2024). Differential cross section with Volkov-thermal wave function in Coulomb potential. Atom Indonesia Journal, 50(1). https://doi.org/10.55981/aij.2024.1309

[19] González de la Cruz, G., and Gurevich, Yu. G. (1996). Electron and photon thermal waves in semiconductors: An application to photothermal effect. Journal of Applied Physics, 80(3), 1726-1727.

[20] Lehman, E. B. (2021). Electrochemistry for materials science. Institute of Metallurgy and Materials Science Polish Academy of Sciences, Poland, Lecture Note.

[21] Kim, B. N. (2022). Angular distribution of electron-helium scattering in the presence of a 1.17 eV laser field (Doctoral dissertation). University of Kentucky, Lexington, KY, United States.

[22] Giri, D. V. (1976). Mathematics notes: One delta function, Part I: A review of various representations and properties of Dirac delta function. Retrieved from http://ece-research.unm.edu/summa/notes/Mathematics/0041.pdf

[23] Masanta, N., and Ghoshal, A. (2021). Dynamics of positron scattering from lithium, sodium and potassium atoms in hot and dense plasmas. Chinese Journal of Physics. https://doi.org/10.1016/j.cjph.2021.01.020

[24] Harris, A. L., Plumadore, A., and Smozhanyk, Z. (2018). Ionization of Hydrogen by Electron Vortex Beam. Journal of Physics B: Atomic, Molecular and Optical Physics, 52, 094001.

[25] Busuladžić, M., Čerkić, A., Odžak, S., Gazibegović-Busuladžić, A., Hasović, E., Habibović, D., and Milošević, D. B. (2014). Atomic and molecular processes generated by linearly polarized few-cycle laser pulses. Physica Scripta, 2014(T162), 014008. https://doi.org/10.1088/0031-8949/2014/T162/014008